ELSEVIER

Journal of Molecular Catalysis A: Chemical 144 (1999) 101–116

JOURNAL OF MOLECULAR CATALYSIS A: CHEMICAL

www.elsevier.com/locate/molcata

A study of manganese-silicoaluminophosphate molecular sieves

A. Vieira [a], M.A. Tovar [a], C. Pfaff [a], P. Betancourt [a], B. Méndez [a], C.M. López [a], F.J. Machado [a], J. Goldwasser [a,*], M.M. Ramírez de Agudelo [b], M. Houalla [c]

[a] *Centro de Catálisis, Petróleo y Petroquímica, Escuela de Química, Facultad de Ciencias, Universidad Central de Venezuela, Apartado Postal 47102, Los Chaguaramos, Caracas 1020-A, Venezuela*

[b] *INTEVEP, Apartado 76343, Caracas 1070-A, Venezuela*

[c] *Department of Chemistry, Vanderbilt University, Nashville, TN 37235, USA*

Received 9 May 1998; accepted 13 September 1998

Abstract

Surface and chemical characterization were performed on a manganese-substituted silicoaluminophosphate molecular sieve (MnAPSO-11), and on a manganese-supported silicoaluminophosphate molecular sieve (Mn/SAPO-11). For comparison purposes, the characterization process was also carried out over the parent SAPO-11 molecular sieve. Different characterization techniques were used: XPS, redox cycles, ^{31}P MAS NMR, and acidity measurements. The transformations of *n*-butane were carried out over the corresponding platinum promoted solids (Pt/MnAPSO-11, Pt/Mn/SAPO-11 and Pt/SAPO-11). Platinum dispersion was measured by H_2 chemisorption. XPS results indicated that manganese was better dispersed on the MnAPSO-11 solid than on the supported Mn/SAPO-11 catalyst. Redox cycles showed a strong difference between the H_2 (or O_2) consumed by each solid. The Mn/SAPO-11 consumed nearly three times as much H_2 (or O_2) per Mn atom as the MnAPSO-11 solid. ^{31}P MAS NMR results showed an increase in the intensity of the side bands, probably due to an anisotropic paramagnetic shift caused by a stronger dipolar interaction between the ^{31}P and the paramagnetic Mn(II) ions on the MnAPSO-11 sample, when compared with the Mn/SAPO-11 solid. These results suggest a better dispersion of the manganese species on the MnAPSO-11 solid, which would facilitate the above mentioned ^{31}P–Mn(II) interaction, in agreement with the XPS results. Acidity was measured by pyridine chemisorption at different temperatures. A larger number of (moderate + strong) Brönsted acid sites was found for the MnAPSO-11 solid compared with the SAPO-11 and Mn/SAPO-11 samples. The addition of platinum decreased the acidity. The Pt dispersions were 83%, 68% and 54% for the Pt/SAPO-11, Pt/Mn/SAPO-11 and Pt/MnAPSO-11 solids, respectively. The catalytic results indicate higher yields for the production of isobutane and isobutene over the Pt/MnAPSO-11. A severe decrease in the yield of formation of hydrocarbons with less than four carbon atoms (undesirable side reaction) was also observed for the Pt/MnAPSO-11 system compared with the Pt/SAPO-11 and Pt/Mn/SAPO-11 systems. An ensemble effect is suggested as responsible for the differences observed in the yield of formation of hydrocarbons with less than four carbon atoms. The higher yield and selectivity observed for the formation of isobutane (iso-C4) and isobutene (iso-C4=) hydrocarbons over the Pt/MnAPSO-11

* Corresponding author. Fax: +1-582-2392162; E-mail: jgoldwas@strix.ciens.ucv.ve

1381-1169/99/$ - see front matter
PII: S1381-1169(98)00338-0

solid, was accounted for in terms of the largest number of (moderate + strong) Brönsted acid sites found on this solid. The catalytic and characterization results suggest the incorporation of manganese into the molecular sieve structure for the substituted MnAPSO-11 solid.

Keywords: *n*-Butane; Mn-silicoaluminophosphates; Molecular sieves; Skeletal isomerization; Dehydrogenation; Platinum; Brönsted acidity; Dehydroisomerization

1. Introduction

Metal-substituted aluminophosphates (MeAPO's) and metal-substituted silicoaluminophosphates (MeAPSO's) molecular sieves have been shown to catalyze a variety of chemical reactions [1–21]. In particular, the incorporation into the synthesis gel of different substitution metal cations such as Cr(III), Mn(II), Ga(III), Zn(II), Fe(II), Co(II), etc. [13–21] has yielded very active and selective catalysts for the skeletal isomerization of *n*-butenes. The high selectivity shown for the formation of isobutene over these solids has been associated with a specific acid site distribution and a particular crystal topology which minimize undesirable side reactions such as cracking and oligomerization.

The importance of isobutene as a valuable feedstock has been well established [22,23] since it can react with methanol, generating methyl *tert*-butyl ether (MTBE), an important octane booster oxygenated fuel additive.

Recently [21], the direct transformation of *n*-butane into isobutene (dehydroisomerization) was performed over platinum promoted Mn-$AlPO_4$-11 molecular sieves. The rationale for this was to explore the possibility of producing isobutene from *n*-butane in a single process, thus avoiding the costs of separate independent reactors (dehydrogenation and acid skeletal isomerization) which are presently used for the manufacture of isobutene [24–29]. In addition, the direct transformation of *n*-butane can also yield appreciable amounts of isobutane, a valuable feedstock used in the production of isooctane (by reaction with *n*-butenes). The results showed that the Pt/MnAPO-11 solid was more selective towards the formation of isobutene and isobutane than the platinum promoted–manganese supported counterpart. Moreover, the formation of C1–C3 hydrocarbons (undesirable side reaction) was seriously hindered over the Pt/MnAPO-11 solid. The catalytic as well as different characterization results strongly suggested the incorporation of Mn(II) into the $AlPO_4$-11 molecular sieve framework for the substituted solid.

The main purpose of the present work is to extend these ideas to a platinum promoted–manganese substituted silicoaluminophosphate molecular sieve (Pt/MnAPSO-11) and to a platinum promoted–manganese supported silicoaluminophosphate molecular sieve (Pt/Mn/SAPO-11). This study will show the effect of Si and Mn addition on the product distribution, for the *n*-butane transformations. X-ray diffraction, ^{31}P magic angle spinning nuclear magnetic resonance spectroscopy (MAS NMR), X-ray photoelectron spectroscopy (XPS), H_2–O_2 redox cycles, acidity measurements (irreversibly chemisorbed pyridine, followed by infrared spectroscopy (IR)) and metallic dispersion measurements (H_2 chemisorption), were used as characterization techniques. The results will provide new evidence for the incorporation of manganese into the framework of molecular sieves with $AlPO_4$-11 (AEL) structure.

2. Experimental

2.1. Catalysts

The synthesis procedure for the parent SAPO-11 has been reported elsewhere [18,19,

30]. The gel molar composition was Al_2O_3:P_2O_5:DPA:0.3SiO_2:50H_2O. The molar composition formula TO_2 for the calcined solid was $(Al_{0.49}P_{0.41}Si_{0.10})O_2$ (SSA = 185 m^2/g).

The synthesis of the MnAPSO-11 was performed according to the following scheme: The alumina source (pseudoboehmite, Catapal B from Vista Chemical) was added to a diluted solution of phosphoric acid (Aldrich), and the mixture was stirred for 2 h. The organic template, (di-*n*-propylamine (DPA) (Aldrich)) was then, followed by a stirring period of 2 h. Thereafter, the source of silicon (40% colloidal silica, Ludox AS40 from Dupont) was added, under vigorous stirring for 2 h. The final step was the addition of the manganese promoter ($Mn(CH_3COO)_2 \cdot 4H_2O$, (Merck)), which was followed by a stirring period of 2 h. The gel molar composition was: 0.9Al_2O_3:P_2O_5:DPA:0.6SiO_2:0.2MnO:40H_2O. A final crystallization temperature of 423 K and a crystallization time of 72 h were employed. The solid was first washed with distilled water and dried at 353 K for 16 h. The catalyst was then calcined under dry air at 773 K for 4 h in order to remove organic residues. The molar composition formula TO_2 for the calcined MnAPSO-11 solid was $(Al_{0.44}P_{0.40}Mn_{0.046}Si_{0.11})O_2$. The Mn wt.% was 3.5 (SSA = 182 m^2/g). A supported Mn/SAPO-11 catalyst was prepared by impregnating a sample of SAPO-11 with the same manganese promoter, using the incipient wetness technique (2.5 wt.% Mn). This sample was then dried and calcined following the procedure described for the MnAPSO-11 catalyst (SSA = 155 m^2/g).

The Pt promoted catalysts were prepared by impregnating the different calcined solids with $[Pt(NH_3)_4(NO_3)_2]$ (BDH, reagent grade) [21,31–33]. The solids were dried under vacuum at 353 K. In order to decompose the Pt complex, the catalysts were calcined under a stream of dry air (30 cm^3/min), using the following procedure: The temperature was increased up to 423 K (5 K/min) followed by a 2 h period at the same temperature. The latter was then increased up to 573 K (5 K/min) and kept constant for 16 h. The Pt loading was 0.5 wt.% Pt for all the Pt promoted solids.

For further experimental details dealing with the preparation and chemical analysis of the catalysts see Refs. [19,21,30].

2.2. Procedures

Specific surface areas were determined on a commercial Micromeritics ASAP 2400 surface area analyzer at liquid nitrogen temperature.

X-ray diffractograms were recorded with a Philips diffractometer PW 1730 using Co $K\alpha$ radiation (λ = 1.790255 Å) operated at 30 kV, 20 mA and scanning speed of 2° (2θ/min).

^{31}P MAS NMR experiments were performed on a Bruker MSL spectrometer, operating at 121.44 MHz for ^{31}P. Other experimental details have been described previously [14,21].

X-ray photoelectron spectra of oxidic and reduced catalysts were obtained with a modified AEI ES200 spectrometer equipped with an aluminum anode (Al $K\alpha$ = 1486.6 eV) at a power of 240 W (12 kV and 20 mA). The instrument was operated in the fixed retardation ratio mode and the analysis pressure was $< 5.10^{-8}$ Torr. The spectrometer was interfaced to an IBM PC compatible for data collection. The subsequent data analysis was also carried out in the PC environment under DOS using programs (GOOGLY software) written in house [34]. Binding energy values (BE) were referenced to the C 1s peak (284.6 eV) from adventitious contamination layer.

The catalysts were pressed and mounted on a sealable probe which allowed transfer of the treated catalyst from an external reaction chamber to the spectrometer without exposure to air (this is particularly important for the reduced samples). The catalysts were treated with oxygen at 773 K for 1 h and transferred to the spectrometer. After data collection, the samples were returned to the reaction chamber, the temperature was ramped up to 773 K in flowing H_2

(100 cc/min) and maintained for 1 h at that temperature. Finally, the reduced samples were returned to the spectrometer for data collection.

The reduction–oxidation (redox) cycles were performed in a conventional BET system identical to that used in Refs. [18,21]. Catalyst samples of approximately 0.4 g were placed in a quartz microreactor and oxidized with pure oxygen (60 cm^3/min) at 773 K. The sample was evacuated ($P < 2 \times 10^{-5}$ Torr) for 1 h at 773 K and cooled to room temperature under vacuum. The catalyst was then exposed to pure hydrogen and the temperature increased (5 K/min) up to 773 K. The hydrogen consumption was measured after 2 h (at 773 K) from the pressure drop due to the reduction process. Care was taken to trap the evolved water (reduction subproduct) at 78 K. The reduced sample was then evacuated for 1 h at 773 K and cooled to room temperature under vacuum. The described experimental sequence was repeated with pure oxygen, yielding the oxygen consumption.

The experimental procedures for the H_2 chemisorption experiments as well as for the chemisorption of pyridine followed by IR spectroscopy, were described previously [21]. They will be repeated here for the sake of completion.

H_2 chemisorption experiments were performed in the BET system mentioned above. Catalyst samples of approximately 0.2 g were placed in a glass microreactor and reduced in situ with pure H_2 (60 cm^3/min) for 2 h at 773 K. After evacuating the catalysts at the same temperature for 1 h, two adsorption isotherms were obtained at room temperature. The linear region of the first isotherm was extrapolated to zero pressure in order to calculate the amount of physisorbed and chemisorbed H_2. After an evacuation period of 1 h, the second isotherm was obtained. The same procedure (as in the first isotherm) was used to calculate the amount of physisorbed H_2. The irreversibly held H_2 was calculated from the difference between both values. A 1:1 H:Pt stoichiometry was assumed to calculate the metallic dispersion (H/Pt) [35,36].

Infrared spectra were recorded at room temperature using a Perkin-Elmer 1760X FTIR spectrometer with a resolution of 2 cm^{-1}. The IR cell described previously [37,38] had a built-in furnace which was used to pretreat samples in situ at high temperatures. The cell could be attached to the BET vacuum system mentioned above. Samples were mounted in the cell as wafers having a thickness of approximately 10–20 mg/cm^2. Before the addition of pyridine, the samples were calcined with pure O_2 (60 cm^3/min) at 773 K for 2 h. The catalysts were then evacuated ($P \leq 2 \times 10^{-5}$ Torr) for 1 h at the same temperature and cooled to room temperature under vacuum.

The pyridine chemisorption experiments were carried out by exposing the pretreated sample to 5 Torr of pyridine vapor for 1 h at 363 K. The wafer was then evacuated for 1 h at different temperatures before the spectra were recorded. The outgassing temperatures used in the present work were: 443 and 623 K. The reason for using these temperatures is to arbitrarily define [18,21] the following acidity regions: moderate + strong (sites retaining pyridine at 623 K) and total (weak + moderate + strong) (sites retaining pyridine at 443 K). Integrated intensities were normalized to unit wafer thickness (mg/cm^2).

n-Butane catalytic transformations were performed in a conventional continuous flow system [18,19,21] operated at atmospheric pressure. Preliminary experiments were carried out to determine the reaction conditions for maximum steady-state formation of isobutene. It should be recalled that the skeletal isomerization is an exothermic reaction while the dehydrogenation of paraffins is an endothermic process. Furthermore, an additional increase in temperature caused a marked deactivation of the catalyst, presumably due to the formation of coke. The reaction parameters used were: Reaction temperature = 773 K, N_2 flow = 15 cm^3/min, H_2 flow = 15 cm^3/min, *n*-butane flow = 3 cm^3/min, weight of catalyst = 1.6 g (WHSV = 0.267 h^{-1}). The reaction products were ana-

lyzed by on-line gas chromatography, using a Hewlett-Packard 5890 A chromatograph with a flame ionization detector. A fused silica KCl/Al_2O_3 column was used for separation purposes. The catalytic tests were performed after the solids were reduced with purified H_2 (60 cm^3/min) at 773 K for 2 h.

2.3. Data treatment

The total conversion (X) was calculated according to Eq. (1)

$$X = \{(\Sigma A_i) - A_{n\text{-butane}}/\Sigma A_i\} \times 100. \quad (1)$$

For a reaction product (or set of products), the selectivity is defined by Eq. (2),

$$S_i = \{A_i/(\Sigma A_i) - A_{n\text{-butane}}\} \times 100, \quad (2)$$

where A_i is the corrected chromatographic area for a particular compound.

The catalytic yield (Y) for the different reaction products is defined by Eq. (3),

$$Y_i = S_i \times X/100 \quad (3)$$

The following selectivities and yields were determined: $S_{\text{iso-C4}}$, $Y_{\text{iso-C4}}$ (formation of isobutane), $S_{n\text{-C4}=}$, $Y_{n\text{-C4}=}$. (formation of *n*-butenes), $S_{\text{iso-C4}=}$, $Y_{\text{iso-C4}=}$ (formation of isobutene), $S_{<\text{C4}}$, $Y_{<\text{C4}}$. (formation of C1–C3 products). Products containing more than four carbon atoms comprised less than 1.5% of the product distribution.

2.4. Reagents

n-Butane was Matheson C.P. grade. Hydrogen was purified by passing it through a molecular sieve and commercial Deoxo traps to remove water and oxygen traces. CO (GIV) was purified according to Ref. [37]. Pyridine (Aldrich, spectrophotometric grade) was degassed using the freeze–pump–thaw technique [39].

3. Results

Fig. 1 shows the XRD diffractogram for the as-synthesized and calcined MnAPSO-11 sample and for the calcined Pt/MnAPSO-11 solid. The diffractogram for the as-synthesized sample (Fig. 1a) shows a highly crystalline solid with $AlPO_4$-11 (AEL) structure, in agreement with the literature [5,21,30]. The major XRD changes observed for the calcined solid (Fig. 1b) have previously been reported [30,40]. They have been associated with a change in the crystal symmetry from a body-centered to a primitive unit cell as a result of water adsorption after calcination. The diffraction pattern shows that the location of the main XRD peaks associated with the calcined MnAPSO-11 catalyst (Fig. 1b), remains unaltered after the addition of platinum to the calcined MnAPSO-11 solid. This result supports the fact that the addition of platinum does not change the crystallographic structure of the calcined MnAPSO-11 solid. Similar results were obtained with the Pt/MnAPO-11 and MnAPO-11 solids [21].

The XRD diffractograms for the as-synthesized and calcined SAPO-11 were shown and discussed previously [30]. The diffractograms are similar to those shown for the as-synthesized and calcined MnAPSO-11 solid, respectively. The addition of platinum to the calcined SAPO-11 catalyst does not modify the crystallographic structure of the latter. No Pt or Mn diffraction peaks were apparent in any of the solids studied in the present work.

XPS P 2p, Al 2p, Si 2p and Mn 2p binding energy (BE) values for calcined and reduced MnAPSO-11 and Mn/SAPO-11 solids are shown in Table 1. It can be readily seen that the P 2p binding energies were essentially constant. The measured value was consistent with that reported for silicoaluminophosphate molecular sieves [41]. Similarly, little variation of the Al 2p BE value was observed. The range of the values obtained (75.2 ± 0.2 eV) was consistent with that reported in Ref. [41]. The Si 2p BE values also varied within the range of experi-

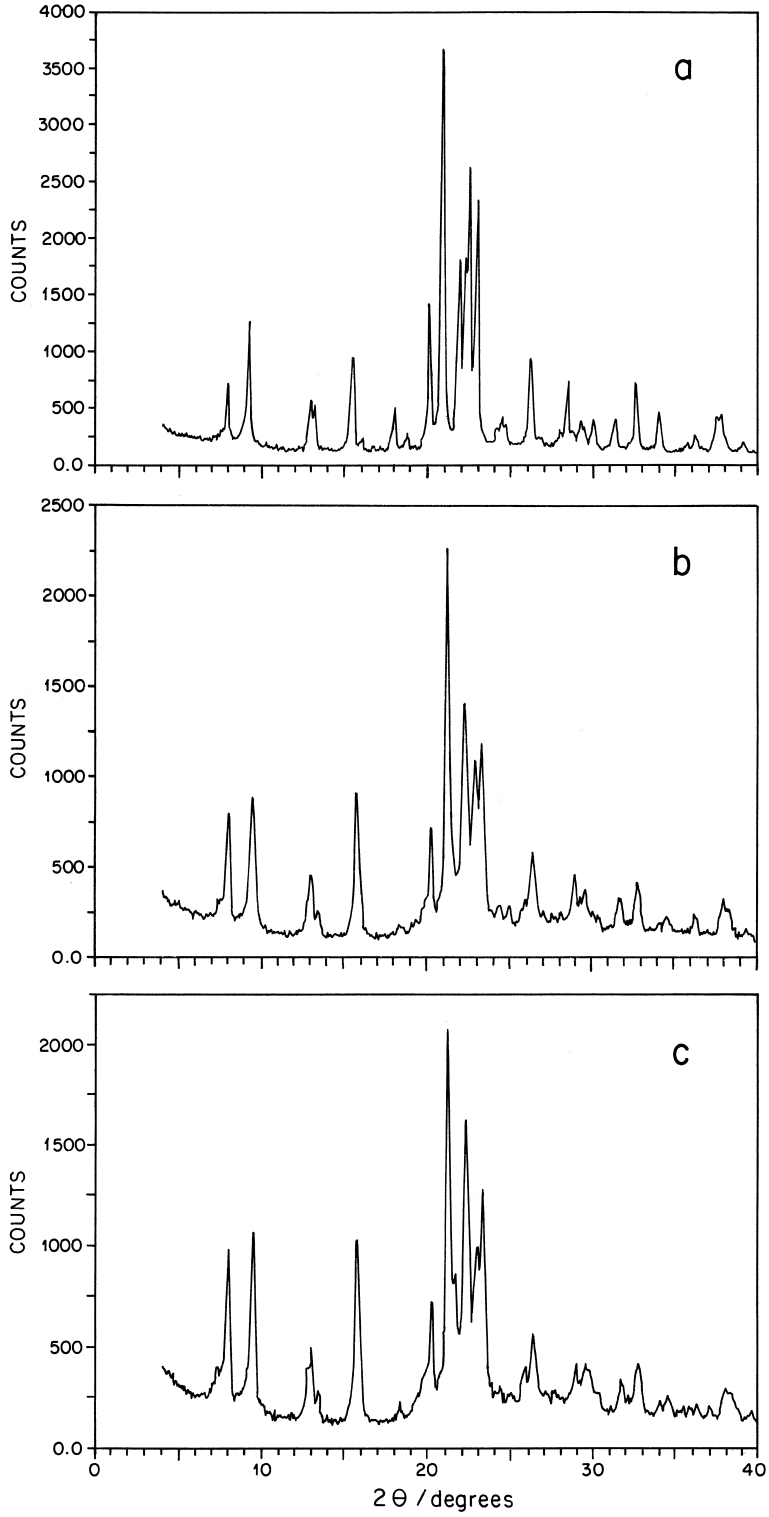

Fig. 1. X-ray diffractogram for: (a) as-synthesized MnAPSO-11 solid, (b) calcined MnAPSO-11 solid (c) calcined Pt/MnAPSO-11 catalyst.

Table 1
XPS results, binding energies and Mn 2p/P 2p intensity ratios

Catalyst	Binding energies (eV)					
	C 1s	Al 2p	P 2p	Mn 2p	Si 2p	Mn 2p/P 2p
MnAPSO-11(oxid.)[a]	284.6	75.2	134.6	642.5	102.8	1.20
MnAPSO-11(red.)[b]	284.6	75.2	134.6	642.5	102.9	1.20
MnSAPO-11(oxid.)[a]	284.6	75.4	134.7	642.7	103.2	0.64
MnSAPO-11(red.)[b]	284.6	75.2	134.6	642.6	103.1	0.63

[a](oxid.) refers to the oxidic solid.
[b](red.) refers to the reduced solid.

mental uncertainty (103.0 ± 0.2 eV). These values were, however, somewhat higher than those reported by Cox and Davis [41] for SAPO molecular sieves. The Mn 2p BE values also varied within a narrow range (642.5 ± 0.2 eV) (Fig. 2). These values are consistent with the

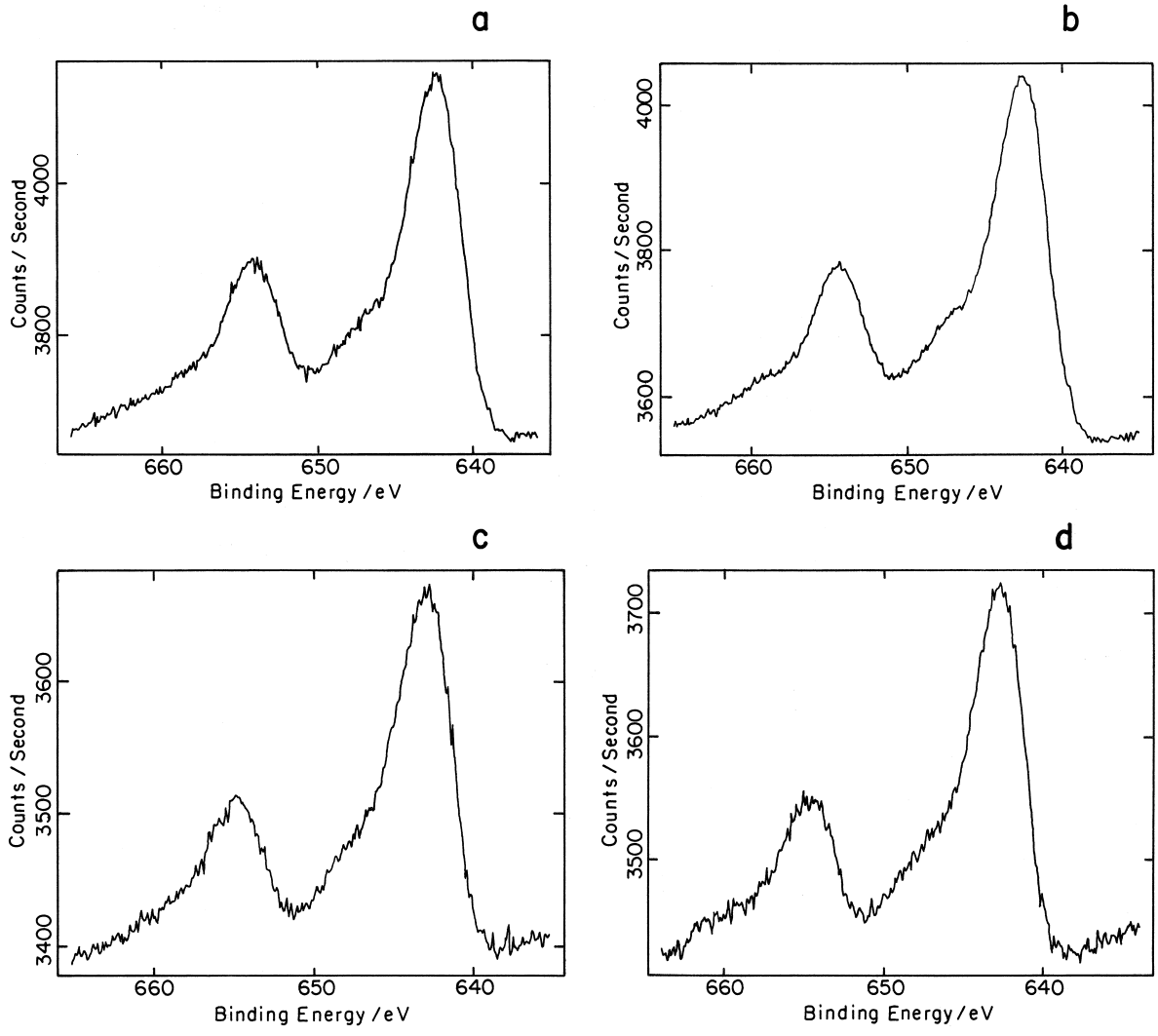

Fig. 2. Mn 2p XPS spectra for: (a) oxidic MnAPSO-11 solid, (b) reduced MnAPSO-11 catalyst, (c) oxidic Mn/SAPO-11 solid, (d) reduced Mn/SAPO-11 catalyst.

Table 2
Results for the reduction–oxidation experiments (H_2–O_2)[a]

Catalyst	$n^{b}_{H_2/g_{cat}}$	$n^{c}_{O_2/g_{cat}}$	H_2/Mn^{d}	O/Mn^{e}
MnAPSO-11	1.15×10^{-4}	6.17×10^{-5}	0.18	0.19
Mn/SAPO-11	2.76×10^{-4}	1.28×10^{-5}	0.61	0.58

[a] The experiments were carried out at 773 K. For more details see Section 2.
[b] Hydrogen consumption in moles of H_2 per g_{cat}.
[c] Oxygen consumption in moles of O_2 per g_{cat}.
[d] H_2 molecules consumed per manganese atom.
[e] Oxygen atoms consumed per manganese atom.

BE value reported for Mn(IV) as in MnO_2 [42]. However, these values may also be indicative of the presence of lower oxidation states arising from well-dispersed manganese species [43]. Fig. 2 also shows the presence of a small shoulder at ca. 648 eV which is slightly more defined for the MnAPSO-11 catalyst than for the Mn/SAPO-11 solid. This shoulder has been previously assigned [44,45] to a small shake-up satellite peak characteristic of paramagnetic Mn(II) species.

Table 1 also shows the corresponding Mn 2p/P 2p intensity ratios. Clearly, for both catalysts, these ratios are not affected by the reduction treatment. This suggests that reduction had very little effect on the manganese dispersion. It can also be readily seen that the Mn 2p/P 2p intensity ratio for the MnAPSO-11 is twofold higher than that of the Mn/SAPO-11 catalyst.

The results for the reduction–oxidation experiments for the MnAPSO-11 and Mn/SAPO-11 solids are shown in Table 2. As observed for each catalyst, the number of hydrogen molecules consumed per manganese atom (H_2/Mn) during the reduction process is almost identical to the number of oxygen atoms consumed per manganese atom (O/Mn) during the oxidation stage. These results indicate that the redox cycles, for each solid, are reversible since a two-electron reduction is produced per each H_2 molecule consumed while a two-electron oxidation is achieved per each oxygen atom consumed. Despite this similarity, the H_2 and O_2

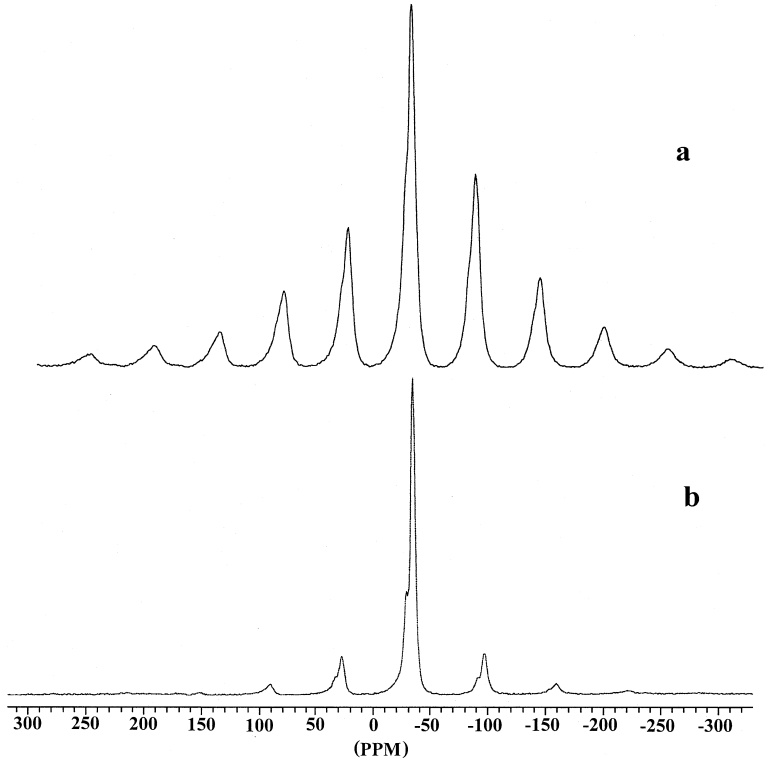

Fig. 3. ^{31}P MAS NMR spectra of: (a) oxidic MnAPSO-11 catalyst, (b) oxidic Mn/SAPO-11 solid.

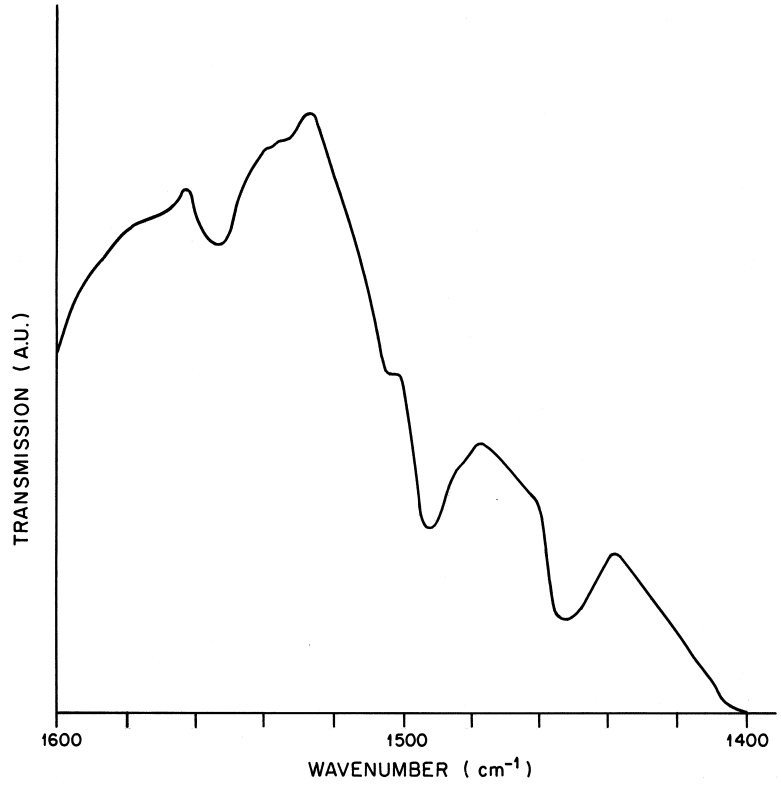

Fig. 4. Infrared spectrum of pyridine adsorbed on the oxidic MnAPSO-11 sample after evacuation at 623 K.

consumptions are extremely different when both solids are compared. The H/Mn (and O/Mn) ratios obtained for the MnAPSO-11 are more than three times lower than those obtained for the Mn/SAPO-11 solid.

Table 3
Normalized integrated intensities for the 1548 cm^{-1} IR band (Brönsted bound pyridine) and for the 1450 cm^{-1} band (Lewis bound pyridine)[a]

Catalyst	Evacuation temperature (K)			
	443		623	
	1548 cm^{-1}	1450 cm^{-1}	1548 cm^{-1}	1450 cm^{-1}
SAPO-11	3.1	3.8	2.8	2.6
MnAPSO-11	5.1	4.2	4.0	3.4
Mn/SAPO-11	2.7	3.9	2.4	2.8
Pt/SAPO-11	2.8	3.4	2.4	2.0
Pt/MnAPSO-11	4.3	3.7	3.5	3.0
Pt/Mn/SAPO-11	2.4	3.2	2.1	2.3

[a] Integrated intensities given in arbitrary units. For more details see text.

Fig. 3 shows the ^{31}P MAS NMR spectra for the MnAPSO-11 and Mn/SAPO-11 samples. Note that for the substituted solid, the intensity of the side bands is strongly enhanced when compared with the supported material, in agreement with previous work [14,21,46].

The IR spectrum for chemisorbed pyridine over the MnAPSO-11 solid evacuated at 623 K is shown in Fig. 4. Similar spectra were obtained for the other solids studied. The spectrum was obtained by subtracting the contribution

Table 4
H_2 uptakes and Pt dispersion measurements[a]

Catalyst	H_2 uptake/ (μmol g)	H/Pt
SAPO-11	n.d[b]	–
Pt/SAPO-11	10.6	0.83
Pt/MnAPSO-11	6.92	0.54
Pt/Mn/SAPO-11	8.71	0.68

[a] For experimental details see text.
[b] n.d—not detected.

Table 5
Product distribution for the transformations of *n*-butane over Pt/SAPO-11[a]

TOS[b]	X	$S_{\text{iso-C4}}$	$S_{\text{iso-C4}=}$	$S_{n\text{-C4}=}$	$S_{<\text{C4}}$	$Y_{\text{iso-C4}}$	$Y_{\text{iso-C4}=}$	$Y_{n\text{-C4}=}$	$Y_{<\text{C4}}$
30	87.4	17.6	5.5	4.5	72.5	15.4	4.8	3.9	63.4
60	79.0	19.7	7.5	7.2	64.5	15.6	5.9	5.7	50.9
90	77.0	19.8	7.2	8.8	62.9	15.2	5.6	6.8	48.4
120	73.3	19.9	7.8	10.9	61.4	14.6	5.7	8.0	45.0
180	68.7	20.8	8.9	12.8	57.5	14.3	6.1	8.8	39.5
300	64.4	21.9	10.3	15.9	51.9	14.1	6.7	10.3	33.4

[a]The reaction parameters used were: reaction temperature = 773 K, N_2 flow = 15 cm^3/min, H_2 flow = 15 cm^3/min, *n*-butane flow = 3 cm^3/min, weight of catalyst = 1.6 g (WHSV = 0.267 h^{-1}).
[b]Time on stream/min.

from the sample before the adsorption of pyridine. The two bands observed at ca. 1450 cm^{-1} and ca. 1548 cm^{-1} have previously been suggested in the literature [39,47] for estimating Lewis and Brönsted acidity on heterogeneous catalysts. The former corresponds to the 19b vibration of the Lewis bound pyridine. The band at ca. 1548 cm^{-1} has been assigned to pyridine adsorbed on Brönsted acid sites. Table 3 summarizes the normalized integrated intensities for the IR bands due to Brönsted and Lewis bound pyridine for catalysts evacuated at 443 and 623 K. It can be observed that the MnAPSO-11 solid presents the highest Brönsted and Lewis acidity, in particular after evacuation of pyridine at 623 K (moderate + strong) acid sites. The Brönsted acidity for the SAPO-11 solid is slightly higher than that obtained for the Mn/SAPO-11 solid. It can also be seen that the addition of Pt causes a slight decrease in the integrated intensity of the IR bands corresponding to Lewis and Brönsted sites, in agreement with reports on related systems [21].

Table 4 summarizes the results for the hydrogen chemisorption experiments. No hydrogen chemisorption was detected for the SAPO-11 solid. The MnAPSO-11 and Mn/SAPO-11 samples did chemisorb a very small amount of H_2, which was negligible compared with the H_2 chemisorbed by the Pt promoted solids. For these solids, the uptake followed the sequence Pt/SAPO-11 > Pt/Mn/SAPO-11 > Pt/MnAPSO-11 catalyst. The Pt dispersion was ~ 51% larger for the Pt/SAPO-11 compared to that observed for the Pt/MnAPSO-11 solid.

n-Butane catalytic tests were carried out over the SAPO-11, MnAPSO-11 and Mn/SAPO-11 solids. The steady state total conversion was always below 2%. The results for the transformation of *n*-butane over the Pt promoted solids

Table 6
Product distribution for the transformations of *n*-butane over Pt/MnAPSO-11[a]

TOS[b]	X	$S_{\text{iso-C4}}$	$S_{\text{iso-C4}=}$	$S_{n\text{-C4}=}$	$S_{<\text{C4}}$	$Y_{\text{iso-C4}}$	$Y_{\text{iso-C4}=}$	$Y_{n\text{-C4}=}$	$Y_{<\text{C4}}$
30	45.0	44.2	16.1	26.8	13.0	19.9	7.3	12.1	5.8
60	43.1	42.9	16.9	28.6	11.5	18.5	7.3	12.3	4.9
100	41.7	41.7	17.7	30.4	10.3	17.4	7.4	12.7	4.3
120	41.0	41.1	17.9	31.0	10.0	16.9	7.3	12.7	4.1
180	39.4	39.1	19.1	32.9	8.9	15.4	7.5	13.0	3.5
300	39.6	38.3	19.2	32.4	10.1	15.2	7.6	12.8	4.0

[a]The reaction parameters used were: reaction temperature = 773 K, N_2 flow = 15 cm^3/min, H_2 flow = 15 cm^3/min, *n*-butane flow = 3 cm^3/min, weight of catalyst = 1.6 g (WHSV = 0.267 h^{-1}).
[b]Time on stream/min.

Table 7
Product distribution for the transformations of *n*-butane over Pt/Mn/SAPO-11[a]

TOS[b]	X	$S_{\text{iso-C4}}$	$S_{\text{iso-C4}=}$	$S_{n\text{-C4}=}$	$S_{<\text{C4}}$	$Y_{\text{iso-C4}}$	$Y_{\text{iso-C4}=}$	$Y_{n\text{-C4}=}$	$Y_{<\text{C4}}$
30	54.4	29.2	9.4	20.1	41.0	15.9	5.1	10.9	22.3
60	48.6	30.8	10.3	23.3	35.6	15.0	5.0	11.3	17.3
90	45.3	31.5	11.2	26.8	29.9	14.3	5.1	12.1	13.5
120	43.0	31.7	11.8	28.5	27.8	13.6	5.1	12.2	11.9
180	41.0	31.2	12.4	31.7	24.7	12.8	5.1	13.0	10.1
310	39.7	31.0	13.0	34.5	20.6	12.3	5.2	13.7	8.2

[a]The reaction parameters used were: reaction temperature = 773 K, N_2 flow = 15 cm^3/min, H_2 flow = 15 cm^3/min, *n*-butane flow = 3 cm^3/min, weight of catalyst = 1.6 g (WHSV = 0.267 h^{-1}).
[b]Time on stream/min.

are shown in Tables 5–7. The most significant feature is the dramatic decrease in the yield and selectivity for the production of C1–C3 hydrocarbons on the Pt/MnAPSO-11 compared to the Pt/SAPO-11 and Pt/Mn/SAPO-11 samples. When compared with the Pt/SAPO-11 sample, the supported Pt/Mn/SAPO-11 solid showed a lower selectivity (and yield) towards the formation of C1–C3 hydrocarbons.

The catalytic results also indicate higher yields for the production of isobutene and isobutane over the Pt/MnAPSO-11 solid, particularly at low times-on-stream (TOS). Similar yields for the production of each iso-C_4 product were observed over the Pt/SAPO-11 and Pt/Mn/SAPO-11 solids.

The yield for the formation of *n*-butenes was similar on both Pt–Mn containing solids. Over the Pt/SAPO-11 catalyst the formation of *n*-butenes was hindered, particularly at low TOS.

For comparison purposes, the catalytic results for the transformations of *n*-butane over a Pt/$AlPO_4$-11 solid are shown in Table 8. This solid does not show any (moderate + strong) Brönsted acidity. Thus, all the reactions involved are metal (Pt) assisted. The results were taken from Ref. [21].

4. Discussion

The characterization results obtained by the different techniques used in the present work, support the incorporation of manganese into the silicoaluminophosphate framework, for the

Table 8
Product distribution for the transformations of *n*-butane over Pt/$AlPO_4$-11[a]

TOS[b]	X	$S_{\text{iso-C4}}$	$S_{\text{iso-C4}=}$	$S_{n\text{-C4}=}$	$S_{<\text{C4}}$	$Y_{\text{iso-C4}}$	$Y_{\text{iso-C4}=}$	$Y_{n\text{-C4}=}$	$Y_{<\text{C4}}$
45	52.5	12.2	6.1	18.7	62.9	6.4	3.2	9.8	33.1
60	50.2	12.3	6.5	21.1	60.0	6.2	3.3	10.6	30.2
90	47.2	11.9	6.9	25.0	56.2	5.6	3.3	11.8	26.5
120	45.5	11.6	7.4	28.0	53.0	5.3	3.4	12.7	24.1
150	41.6	12.2	6.9	29.5	51.4	5.1	2.9	12.3	21.4
180	41.7	11.6	7.2	30.3	50.8	4.8	3.0	12.6	21.2
240	43.5	11.1	7.5	32.4	49.1	4.8	3.3	14.1	21.3
300	40.1	10.3	7.7	35.6	46.4	4.2	3.1	14.3	18.6

[a]The reaction parameters used were: reaction temperature = 773 K, N_2 flow = 15 cm^3/min, H_2 flow = 15 cm^3/min, *n*-butane flow = 3 cm^3/min, weight of catalyst = 1.6 g (WHSV = 0.267 h^{-1}). The data were taken from Ref. [21].
[b]Time on stream/min.

MnAPSO-11 (and Pt/MnAPSO-11) solids. The reasons are the following:

A. The different results obtained in the redox experiments for the substituted and supported materials. As shown in Table 2, the manganese species present in the MnAPSO-11 solid show a much higher stability towards reduction–oxidation than the corresponding species of the Mn-supported solid. In fact, the latter shows a similar redox behavior than that observed for manganese–alumina catalysts, prepared by pore volume impregnation of the support with $Mn(NO_3)_2$ [43]. These impregnated catalysts, consisted primarily in manganese oxide [Mn(III) and Mn(IV)] microcrystals 2–4 nm in size deposited mainly at the outer region of the alumina particles [43]. On the other hand, if Mn(II) is incorporated into the molecular sieve framework, it should be more difficult to oxidize and reduce than the manganese species present in the above mentioned $Mn(NO_3)_2$/alumina catalysts. The small values obtained for the H_2 (or O_2) consumption over the MnAPSO-11 solid may indicate that a small fraction of manganese was not incorporated in this case, as suggested for the related MnAPO-11 solid [21].

B. The XPS results indicate that the Mn 2p/P 2p intensity ratios for the Mn-substituted solid are larger by a factor of two than the corresponding ratios for the supported catalyst Mn/SAPO-11. The observed differences in the intensity ratios cannot be fully accounted for by the difference in Mn content (2.5 wt% for the Mn-supported solid and 3.5 wt% for the MnAPSO-11 catalyst). Thus, it can be concluded that the manganese species on the MnAPSO-11 solid are better dispersed than those present on the supported solid. In addition, the intensity ratios for the oxidic and reduced MnAPSO-11 samples were identical. Thus, the sample appeared to be little affected by the reduction–oxidation treatment, as observed for a CrAPSO-11 sample [18]. These results are consistent with the notion of Mn(II) being incorporated in the MnAPSO-11 solid. It should be noted, however, that the Mn 2p/P 2p intensity ratios observed for the oxidic and reduced Mn-supported system were also similar. This suggests that no significant redispersion or aggregation occurs upon reduction of Mn oxide-type species, as observed for related systems [18].

C. ^{31}P MAS NMR spectra (Fig. 3), which show differences in the intensity of the side bands for the substituted and supported samples, in accordance with previous reports [14,21,46]. An anisotropic paramagnetic shift due to a ^{31}P–paramagnetic Mn(II) dipolar interaction, for the MnAPSO-11 catalyst, has been suggested to account for the observed differences. These results suggest a better dispersion of the manganese species on the MnAPSO-11 solid, which would facilitate the abovementioned ^{31}P–Mn(II) interaction. The ^{31}P MAS NMR results are in agreement with the XPS data (intensity ratios).

D. The increased (moderate + strong) Brönsted acidity shown by the MnAPSO-11 catalyst (Table 3) compared with the parent SAPO-11 and with the supported Mn/SAPO-11 solids. Particularly, the difference in acidity between the substituted and supported manganese catalysts is significant since the latter should contain predominantly extra-framework manganese species. The appearance of these species does not create new (moderate + strong) Brönsted acid sites, compared with the SAPO-11 sample. The situation with the MnAPSO-11 solid is clearly different. This can be accounted for in terms of the incorporation of Mn(II) into the silicoaluminophosphate structure (MnAPSO-11) by replacement of an Al(III) cation, as proposed by Gielgens et al. [48]. According to these ideas, Mn(II) would be incorporated into the molecular sieve framework generating one P–OH group per each metal ion, thus increasing the number of acid sites. The interaction of the metal ions (Lewis centers) with the P–OH groups (Brönsted sites) may increase the strength of the latter, as shown for related systems [14,18,21]

The above-mentioned results (points A through D), support the assumption of Mn(II)

being incorporated into the silicoaluminophosphate molecular sieve structure, in agreement with other studies [21]. However, the presence of some extra-framework manganese species on the substituted solid cannot be ruled out., viz, our data does not allow us to conclude that all the manganese is incorporated into the molecular sieve structure, for the MnAPSO-11 solid.

The acidity of the catalysts (Brönsted and Lewis sites) is decreased by the addition of Pt, in agreement with results obtained over Pt/SAPO-11 catalysts [49] and over Pt/$AlPO_4$-11 catalysts [21]. The Pt dispersion, measured by the irreversibly chemisorbed hydrogen, was 54% for the Pt/MnAPSO-11, 68% for the Pt/Mn/SAPO-11 and 83% for the Pt/SAPO-11 solid. Besides the numerical implications, these results show that the presence of manganese decreases the amount of hydrogen held by the platinum particles. A close proximity between Pt and manganese species, which may shield a fraction of the 'accessible' platinum crystallites can, therefore, be suggested, in particular for the well dispersed Mn sample (Pt/MnAPSO-11). These ideas will be supported by the catalytic results, vide infra.

The results for the *n*-butane transformations reported in Tables 5–7 are consistent with the acidity and dispersion measurements. The most notable difference, is the dramatic decrease in the yield (and selectivity) for the formation of C1–C3 hydrocarbons, undesired side reaction, for the Pt/MnAPSO-11 solid compared with the Pt/SAPO-11 and Pt/Mn/SAPO-11 catalysts. The formation of lower hydrocarbons can either be acid catalyzed (acid cracking) [50] and/or metal assisted (hydrogenolysis reaction) [36]. Our results support the idea that Pt plays a major role in the formation of C1–C3 hydrocarbons due to the following: It can be observed that the most acidic catalyst (Pt/MnAPSO-11) is the least active catalyst for the formation of lower hydrocarbons. Moreover, the other two platinum containing solids exhibited similar (moderate + strong) Brönsted acid sites, while showing different yields towards the formation of C1–C3 hydrocarbons. In addition, Table 8 shows the catalytic results obtained over the Pt/$AlPO_4$-11 catalyst [21], under the same experimental conditions than those used in the present work. It was shown that this solid has no Brönsted acidity necessary to perform the cracking reaction by an acid mechanism. Thus, it can be safely assumed that the C–C bond breakage occurs on the Pt surface of the Pt/$AlPO_4$-11 solid. The results of Table 8 indicate that the most favored reaction is the hydrogenolysis transformation. Moreover, even though there are no (moderate + strong) Brönsted acid sites on the Pt/$AlPO_4$-11 solid, the yields for the hydrogenolysis reaction are higher than those observed for the Pt/Mn/SAPO-11 and Pt/MnAPSO-11 catalysts (where (moderate + strong) Brönsted acidity is present).

From the above discussion it follows that the hydrogenolysis reaction occurring on the Pt metal surface is a major contributor for the formation of C1–C3 hydrocarbons, over the catalysts used in the present work. The data however does not allow us to totally neglect the formation of a certain amount of C1–C3 hydrocarbons stemming from an acid cracking mechanism.

The hydrogenolysis reaction has been thoroughly investigated [36] over a variety of metallic surfaces. It is now widely accepted that this reaction is structure sensitive and that metallic ensembles over a certain size are needed for the reaction to occur. The decrease in the yields for the hydrogenolysis reaction observed for the Pt/MnAPSO-11 can, in principle, be attributed to an ensemble effect, an electronic effect, or to both. In a previous study [21], it was shown that the Pt electron density was quite similar in the Pt/$AlPO_4$-11 and Pt/MnAPO-11 solids, viz, the electronic properties of the Pt particles were not significantly affected by the presence of the manganese species. Taking these results into consideration, an ensemble effect would be favoured to explain the decrease in the yields for the hydrogenolysis reaction over the MnAPSO-11 catalyst. The latter is supported by

the decrease in the Pt dispersion (observed for the Pt/MnAPSO-11 solid) and it is made possible by the close proximity between Pt crystals and well-dispersed manganese species discussed above.

It can also be observed that the yields for the hydrogenolysis reaction on the supported Pt/Mn/SAPO-11 catalyst are also lower than those observed for the Pt/SAPO-11. However, the decrease is smaller compared with that observed for the Pt/MnAPSO-11 solid. A possible explanation could be that in the case of the supported catalyst, the extra-framework manganese species are poorly dispersed (compared with the substituted solid), as shown by the XPS intensity ratios, thus decreasing the likelihood of manganese species 'seeing' the platinum particles. The difference in Pt dispersion between the supported and substituted molecular sieves, as well as the NMR results obtained for the MnAPSO-11 and Mn/SAPO-11 solids, support the above ideas.

Another important observed catalytic feature, is that the $Y_{\text{iso-c4}}$ and $Y_{\text{iso-C4=}}$ obtained for the Pt/MnAPSO-11 catalyst are higher than those obtained for the Pt/SAPO-11 and Pt/Mn/SAPO-11 solids, particularly at low TOS. The last two solids showed similar yields towards the formation of each iso-C4 product. These results are in line with the acidity measurements shown in Table 3. However, skeletal isomerization of paraffins over heterogeneous catalysts is known to take place by either acid catalysis [50] or by a metal assisted process [36]. Particularly, Pt has been shown to be extremely active for the isomerization process. Due to the presence of both functions on all catalysts studied, the interpretation of the results obtained is more complicated. In this case, in addition to the isomerization–dehydrogenation process carried out over metallic centers, which has been shown to occur over a non-acidic Pt/$AlPO_4$-11 solid (Table 8), the conventional bifunctional mechanism also takes place to produce isobutene + isobutane [51–56]. This mechanism includes: dehydrogenation of *n*-butane to form *n*-butenes, skeletal isomerization of the olefin over (moderate + strong) Brönsted acid sites to yield isobutene followed by a hydrogenation step to form isobutane.

5. Conclusions

XPS results indicated that manganese was better dispersed on the MnAPSO-11 solid than on the supported Mn/SAPO-11 catalyst. Redox cycles showed a strong difference between the H_2 (or O_2) consumed by each solid. The Mn/SAPO-11 consumed nearly three times as much H_2 (or O_2) per Mn atom, as the MnAPSO-11 solid. ^{31}P MAS NMR results showed an increase in the intensity of the side bands, probably due to an anisotropic paramagnetic shift caused by a stronger dipolar interaction between the ^{31}P and the paramagnetic Mn(II) ions on the MnAPSO-11 sample, when compared with the Mn/SAPO-11 solid. These results suggest a better dispersion of the manganese species on the MnAPSO-11 solid, which would facilitate the abovementioned ^{31}P–Mn(II) interaction, in agreement with the XPS results. Acidity was measured by pyridine chemisorption at different temperatures. A larger number of (moderate + strong) Brönsted acid sites was found for the MnAPSO-11 solid compared with the SAPO-11 and Mn/SAPO-11 samples.

The addition of platinum decreased the acidity. The Pt dispersions were 83%, 68% and 54% for the Pt/SAPO-11, Pt/Mn/SAPO-11 and Pt/MnAPSO-11 solids, respectively. The catalytic results indicate higher yields for the production of isobutane and isobutene over the Pt/MnAPSO-11. A severe decrease in the yield of formation of hydrocarbons with less than four carbon atoms (undesirable side reaction) was also observed for the Pt/MnAPSO-11 system compared with the Pt/SAPO-11 and Pt/Mn/SAPO-11 systems.

An ensemble effect is suggested as responsible for the differences observed in the yield of formation of hydrocarbons with less than four

carbon atoms. The higher yield and selectivity observed for the formation of iso-C4 and iso-C4= hydrocarbons over the Pt/MnAPSO-11 solid, was accounted for in terms of the largest number of (moderate + strong) Brönsted acid sites found on this solid.

The catalytic and characterization results suggest the incorporation of manganese into the molecular sieve structure for the substituted MnAPSO-11 solid.

Acknowledgements

The authors would like to express their gratitude to Consejo Nacional de Investigaciones Científicas y Tecnológicas (CONICIT) and Consejo de Desarrollo Científico y Humanístico de la Universidad Central de Venezuela (CDCH-UCV) for financial support, through Grants RPI-10001 and 03-12-3876-97, respectively.

References

[1] S.T. Wilson, B.M. Lok, C.A. Messina, R.T. Gajek, R.L. Patton, E.M. Flanigen, J. Am. Chem. Soc. 104 (1982) 1146.
[2] E.M. Flanigen, B.M. Lok, R.L. Patton, S.T. Wilson, Pure Appl. Chem. 58 (1986) 1351.
[3] E.M. Flanigen, R.L. Patton, S.T. Wilson, in: P.J. Grobert, W.J. Mortier, E.F. Vansant, G. Schulz-Ekloff (Eds.), Innovation in Zeolite Materials Science, Elsevier, Amsterdam, 1988, p. 13.
[4] E.M. Flanigen, B.M.T. Lok, R.L. Patton, S.T. Wilson, US Pat. 4,759,919, 1988.
[5] E.M. Flanigen, B.M.T. Lok, R.L. Patton, S.T. Wilson, US Pat. 4,738,837, 1988.
[6] G.A. Ozin, A. Kuperman, A. Stein, Angew. Chem. 101 (1989) 373.
[7] J.B. Parise, Stud. Surf. Sci. Catal. 24 (1985) 271.
[8] J.D. Chen, R.A. Sheldon, J. Catal. 153 (1995) 1.
[9] N. Rajic, D. Stojakovic, S. Hocevar, V. Kaulic, Zeolites 13 (1993) 384.
[10] B.M. Weckhuysen, R.A. Schoonheydt, Zeolites 14 (1994) 360.
[11] J.D. Chen, J. Dakka, E. Neeleman, R.A. Sheldon, J. Chem. Soc., Chem. Commun. 1379 (1993) .
[12] D. Arias, A. Colmenares, M.L. Cubeiro, J. Goldwasser, C.M. López, F.J. Machado, V. Sazo, Catal. Lett. 45 (1997) 51.
[13] L.H. Gielgens, I.H.E. Veenstra, V. Ponec, M.J. Haanepen, J.H.C. van Hooff, Catal. Lett. 32 (1995) 195.
[14] D. Arias, I. Campos, D. Escalante, J. Goldwasser, C.M. López, F.J. Machado, B. Méndez, D. Moronta, M. Pinto, V. Sazo, M.M. Ramírez de Agudelo, J. Mol. Catal. 122 (1997) 175.
[15] H.-L. Zubowa, M. Richter, U. Roost, B. Parlitz, R. Fricke, Catal. Lett. 19 (1993) 67.
[16] S.M. Yang, D.H. Guo, J.S. Lin, G.T. Wang, Zeolites and Related Microporous Materials: State of the Art 1994, in: J. Weitkamp, H.G. Karge, H. Pfeifer, W. Hölderich (Eds.), Studies in Surface Science and Catalysis, Vol. 84, Elsevier, Amsterdam, 1994, p. 1677.
[17] D. Escalante, J. Goldwasser, C.M. López, F.J. Machado, M, Pinto, M.M. Ramírez-Agudelo, in: E. Herrero, O. Anunziata, C. Pérez (Eds.), Proceedings of the XV Iberoamerican Symposium on Catalysis, Vol. 1, Córdoba, Argentina, 1996, p. 103.
[18] D. Escalante, L. Giraldo, M. Pinto, C. Pfaff, V. Sazo, M. Matjushin, B. Méndez, C.M. López, F.J. Machado, J. Goldwasser, M.M. Ramírez de Agudelo, J. Catal. 169 (1997) 176.
[19] F.J. Machado, C.M. López, J. Goldwasser, B. Méndez, Y. Campos, D. Escalante, M. Tovar, M.M. Ramírez de Agudelo, Zeolites 19 (1997) 387.
[20] D. Escalante, B. Méndez, G. Hernández, C.M. López, F.J. Machado, J. Goldwasser, M.M. Ramírez de Agudelo, Catal. Lett. 47 (1997) 229.
[21] A. Vieira, M.A. Tovar, C. Pfaff, B. Méndez, C.M. López, F.J. Machado, J. Goldwasser, M.M. Ramírez de Agudelo, J. Catal. 177 (1998) 60.
[22] M.W. Simon, S.L. Suib, Chi-Lin. O'Young, J. Catal. 147 (1994) 484.
[23] I.E. Maxwell, J.E. Naber, Catal. Lett. 12 (1992) 105.
[24] E.B. Cornelius, D.W. Koester, US Pat. 3,665,049, 1972.
[25] E.S Tomezsco, US Pat. 3,697,614, 1972.
[26] F. Buonomo, R. Jezzi, B. Notari, G.R. Kotelnikov, UK Pat. GB 2,177,317A, 1987.
[27] E.J. Kuhlman, J.R. Pascoe, C.J. Thom, US Pat. 5,463,160, 1995.
[28] M.R. Apellan, I. Rahmim, A.S. Fung, A. Huss, US Pat. 5,321,194, 1994.
[29] P.T. Barger, R.L. Patton, D.A. Lesch, L.J. Bauer, G.J. Gajda, US Pat. 5,365,008, 1996.
[30] M. Alfonzo, J. Goldwasser, C.M. López, F.J. Machado, M. Matjushin, B. Méndez, M.M. Ramírez de Agudelo, J. Mol. Catal. 98 (1995) 35.
[31] A.C.M. Van den Broek, J. van Grondelle, R.A. van Santen, J. Catal. 167 (1997) 417, See references therein.
[32] W.M.H. Sachtler, Z. Zhang, Adv. Catal. 39 (1993) 129.
[33] S.T. Homeyer, W.M.H. Sachtler, J. Catal. 117 (1989) 91.
[34] GOOGLY Software, copyright 1994 Andrew Proctor, all rights reserved.
[35] D.J. O'Rear, D.G. Loffler, M. Boudart, J. Catal. 121 (1990) 131.
[36] V. Ponec, G.C. Bond., Catalysis by Metals and Alloys, Studies in Surface Science and Catalysis, Vol. 95, Elsevier, Amsterdam, 1995.
[37] J. Goldwasser, M. Houalla, S.M. Fang, W.K. Hall, J. Catal. 115 (1989) 34.

[38] M.R. Goldwasser, D. Rojas, J. Goldwasser, J. Catal. 135 (1992) 596.
[39] K. Segawa, W.K. Hall, J. Catal. 76 (1982) 133.
[40] N. Tapp, N. Milestone, M. Bowden, R. Meinhold, Zeolites 10 (1990) 105.
[41] D.F. Cox, M.E. Davis, Novel Materials in Heterogeneous Catalysis, The American Chemical Society, 1990, pp. 38.
[42] D. Briggs, M.P. Seah (Eds.) Practical Surface Analysis, 2nd edn., Vol. 1, Wiley, New York, 1995.
[43] F. Kapteijn, A.D. van Langeveld, J.A. Moulijn, A. Andreini, M. A Vuurman, A.J. Turek, J.-M. Jehng, I.E. Wachs, J. Catal. 150 (1994) 94.
[44] V. Di Castro, G. Polzonetti, J. Electron. Spectrosc. Relat. Phenom. 48 (1989) 117.
[45] M. Oku, K. Hirokawa, J. Electron. Spectrosc. Relat. Phenom. 7 (1975) 465.
[46] Z. Olender (Levi), D. Goldfarh, J. Batista, J. Am. Chem. Soc. 115 (1993) 1106.
[47] F.E. Kiviat, L. Petrakis, J. Phys. Chem. 77 (1973) 1232.
[48] L.H. Gielgens, I.H.E. Veenstra, V. Ponec, M.J. Haanepen, J.H.C. van Hooff, Catal. Lett. 32 (1995) 195.
[49] J.M. Campelo, F. Lafont, J.M. Marinas, J. Catal. 156 (1995) 11.
[50] A. Corma, B. Wojciechowski, Catal. Rev. Sci. Eng. 24 (1982) 1.
[51] G.A. Mills, H. Heinemann, T.H. Milliken, A.G. Oblad, Ind. Eng. Chem. 45 (1953) 134.
[52] J.H. Sinfelt, H. Hurwitz, J.C. Rohrer, J. Phys. Chem. 64 (1960) 892.
[53] P.B. Weisz, Adv. Catal. 13 (1962) 137.
[54] F. Alvarez, F.R. Ribeiro, G. Giannetto, F. Chevalier, G. Pérot, Guisnet, M., Zeolites, facts, figures, future, in: P.A. Jacobs, R.A. van Santen, (Eds.), Studies in Surface Science and Catalysis, Vol. 49, Elsevier, Amsterdam, 1989, p. 1339.
[55] J. Weitkamp, S. Ernst, Catal. Today 3 (1987) 451.
[56] Ch.N. Satterfield, Heterogeneous Catalysis in Practice, McGraw-Hill, New York, 1980.